Soft Matter

Cosolvent incorporation modulates the thermal and structural response of PNIPAM/silyl methacrylate copolymers

Journal:	*Soft Matter*
Manuscript ID	SM-ART-02-2024-000246.R1
Article Type:	Paper
Date Submitted by the Author:	17-Mar-2024
Complete List of Authors:	Linn, Jason; University of Minnesota Twin Cities, Chemical Engineering and Materials Science Rodriguez, Fabian; The University of Texas Rio Grande Valley, Mechanical Engineering Calabrese, Michelle; University of Minnesota System, Chemical Engineering and Materials Science;

Journal Name

ARTICLE TYPE

Cite this: DOI: 00.0000/xxxxxxxxxx

Cosolvent incorporation modulates the thermal and structural response of PNIPAM/silyl methacrylate copolymers†

Jason D. Linn, Fabian A. Rodriguez, and Michelle A. Calabrese*

Received Date
Accepted Date

DOI: 00.0000/xxxxxxxxxx

Polymers functionalized with inorganic silane groups have been used in wide-ranging applications due to the silane reactivity, which enables formation of covalently-crosslinked polymeric structures. Utilizing stimuli-responsive polymers in these hybrid systems can lead to smart and tunable behavior for sensing, drug delivery, and optical coatings. Previously, the thermoresponsive polymer poly(*N*-isopropyl acrylamide) (PNIPAM) functionalized with 3-(trimethoxysilyl)propyl methacrylate (TMA) has demonstrated unique aqueous self-assembly and optical responses following temperature elevation. Here, we investigate how cosolvent addition, particularly ethanol and *N,N*-dimethyl formamide (DMF), impacts these transition temperatures, optical clouding, and structure formation in NIPAM/TMA copolymers. Versus purely aqueous systems, these solvent mixtures can introduce additional phase transitions and can alter the two-phase region boundaries based on temperature and solvent composition. Interestingly, TMA incorporation strongly alters phase boundaries in the water-rich regime for DMF-containing systems but not for ethanol-containing systems. Cosolvent species and content also alter the aggregation and assembly of NIPAM/TMA copolymers, but these effects depend on polymer architecture. For example, localizing the TMA towards one chain end in 'blocky' domains leads to formation of uniform micelles with narrow dispersities above the cloud point for certain solvent compositions. In contrast, polydisperse aggregates form in random copolymer and PNIPAM homopolymer solutions – the size of which depends on solvent composition. The resulting optical responses and thermoreversibility also depend strongly on cosolvent content and copolymer architecture. Cosolvent incorporation thus increases the versatility of inorganic-functionalized responsive polymers for diverse applications by providing a simple way to tune the structure size and optical response.

1 Introduction

Stimulus-responsive polymers can undergo drastic changes in conformation in response to external stimuli, including temperature,[1] pH,[2–4] and radiation,[5] among others,[6] which can be harnessed to create functional systems for applications such as drug delivery,[7–9] sensing,[10–12] chemical separations,[13] and water remediation.[14,15] Stimuli-responsive polymers can demonstrate responses in systems such as polymer solutions,[16] micelles,[17] gels from the nano through macro scales,[7,9,18,18–24] grafted nanoparticles,[25,26] and surface brushes[27] – in other words, the response can be robust over a wide range of processing conditions and polymer structures.

One of the most widely studied thermoresponsive polymers is poly(*N*-isopropyl acrylamide) (PNIPAM). Aqueous PNIPAM exhibits a lower critical solution temperature (LCST), below which the polymer chains are miscible with the solvent and form hydrated coils. Above a critical temperature, typically near 35 °C, a two-phase region results when the polymer chains change conformation from hydrated coils to collapsed chains. These collapsed chains then aggregate into globules corresponding with a clouding of the solution. Aqueous PNIPAM exhibits a type II LCST behavior, where this critical temperature is largely insensitive to both polymer concentration and molecular weight.[28] This lack of transition temperature tunability for aqueous PNIPAM homopolymer limits its utility for applications requiring responsiveness outside of a few-degree range.

Numerous stimuli-responsive polymeric materials for applications utilizing coatings and nanoparticles require well-controlled polymer structure sizes to attain high performance or to achieve a particular function.[29,30] The size of structures and features formed by responsive polymers largely dictate properties in ap-

421 Washington Ave SE, Minneapolis, MN 55455, USA. E-mail: mcalab@umn.edu; Tel: +612-625-2551

† Electronic Supplementary Information (ESI) available: [details of any supplementary information available should be included here]. See DOI: 00.0000/00000000.

plication. For example, the size of nanostructures used for drug delivery influences the release properties and the biological transport of such systems,[30,31] making structure size a critical parameter to control. In systems such as passive smart windows made with responsive polymer hydrogels, topological restructuring can lead to changes in opacity, where structures large enough to substantially scatter sunlight must form at high temperatures.[24] While the thermoresponsive properties of PNIPAM are desirable for these and other applications, PNIPAM homopolymer forms large, polydisperse aggregates at elevated temperatures,[32] further limiting its practicality in advanced materials.

To enable greater control over the transition temperatures and structuring at high temperatures of PNIPAM, a change the responsive moiety[1] or copolymerization can be used.[32–34] Beyond altering the polymer chemistry and structure, external additives can alter the thermal response and structuring of aqueous PNIPAM. Common additives include salts, surfactants, and organic small molecules.[35–37] However, surfactants can worsen coating quality and salts can lead to corrosion, potentially limiting applications.[38–40] As such, organic solvent incorporation is of particular interest here as a simple and versatile method to alter the response and structure formation of PNIPAM-containing polymers.

PNIPAM in binary solvent systems of water mixed with an organic solvent can exhibit complex behavior, where the mixture of two individual good solvents can lead to regions of immiscibility, also known as co-nonsolvency.[41] While the specifics of the phase diagram are unique to each solvent, in general, addition of a cosolvent decreases the transition temperature in the water-rich regime. Upon increasing the solvent, the transition temperature may sharply increase, leading to miscibility across all experimentally accessible temperatures (as is the case for acetone and methanol, among numerous others), or there may be an upper critical solution temperature (UCST) boundary, below which the polymer is immiscible (as is the case for *N,N*-dimethyl formamide (DMF), ethanol (EtOH), and dimethyl sulfoxide). In systems that display both an LCST and UCST, there can be a region where PNIPAM is immiscible across all temperatures. Numerous studies have attempted to probe the origins of co-nonsolvency, with explanations including changes in the energetics of the bulk solvent[42] and specific polymer/solvent interactions.[43]

While there are competing theories as to the origin of co-nonsolvency, the phenomenon can also be harnessed during synthesis and processing to create particles, gels, and coatings with distinct properties.[11,44,45] Especially when stabilized onto surfaces, the polymer conformation during processing can drastically impact the function of the coatings. Matsuguchi and Fujii[11] fabricated a hydrogen chloride gas detector using PNIPAM microparticles cast from co-nonsolvent water/methanol and found a greater response and recovery compared to microparticles cast from pure water. These differences were attributed to a more heterogeneous coating structure from the co-nonsolvent system leading to increased contact between the coating and the sensor, thus augmenting the sensitivity. Yakushiji *et al.*[46] studied the thermoresponsive function of PNIPAM-modified surfaces, and found that the chain conformation during grafting played an important role in the function of the coatings. Coatings made from poorer solvents showed a greater thermal response in comparison to good solvents. These differences are attributed to the decreased chain mobility in the coatings prepared from good solvents, as the chains are extended on the surface, limiting the extent of the conformation change. Additionally, co-nonsolvency has been utilized to impart additional function to polymer brushes for nanoparticle separations, where the different brush conformations and surface adhesion can be accessed by varying the solvent environment as opposed to temperature.[47] Controlling the solvent composition has also been demonstrated as a method to alter the permeability of responsive polymer-containing membranes.[48] Thus, co-nonsolvency can be exploited not only to tune the properties of a responsive polymer by altering the structure during processing, but also as a means to actively operate the processed polymers in applications.

Prior work from Linn *et al.*[32] investigated PNIPAM copolymers with 3-(trimethoxysilyl)propyl methacrylate (TMA) as a route for controlling the structure size. A critical advantage to this system is that the TMA group enables post-synthetic surface grafting and inter-chain crosslinking, which is critical in numerous applications to stabilize the polymer structures and prevent structural breakup into single polymer chains.[24,49,50] However, to maintain long-term function in applications such as sensing, chemical separations, and smart windows, reversibility of the stimulus response and the polymer mobility must be maintained. Polymers with high TMA (and similar alkoxysilane-containing monomers) content are difficult to produce with acceptable dispersities, so copolymerization with acrylamides or acrylates is common.[50–52] Even with the approach of copolymerization, copolymers containing TMA often display poor thermal reversibility due to the intermolecular silane crosslinking, in effect, any thermal response from the PNIPAM components of a P(NIPAM-*co*-TMA) copolymer is limited to only one cycle. Linn *et al.*[32] demonstrated that localizing the TMA-containing polymer to one chain end can lead to greater cyclability in copolymers of NIPAM and TMA, which could be advantageous in applications requiring responses over multiple thermal cycles. Additionally, in contrast to random copolymers, which formed large and disperse structures ($\approx$ 200-400 nm) at high temperatures, polymers with localized TMA formed small, uniform micellar structures ($\approx$ 100-200 nm).

As both comonomer and cosolvent incorporation can be used to tailor the response of PNIPAM, we investigate the effects of incorporating organic cosolvents on the optical response and the structure sizes formed above the transition temperature of aqueous poly(*N*-isopropyl acrylamide-co-3-(trimethoxysilyl)propyl methacrylate) (P(NIPAM-*co*-TMA)). Given the uniform structure assembly observed in aqueous P(NIPAM-*co*-TMA) with localized TMA,[32] tuning the responses with cosolvents can increase the potential applications for these uniquely behaving systems. Here, the primary cosolvents examined include ethanol and DMF; these solvents were selected as the ternary systems of PNIPAM/water/EtOH and PNIPAM/water/DMF both demonstrate LCST and UCST behavior, but at substantially different cosolvent incorporation. EtOH and DMF have also been shown to localize at the collapsed polymer; however, these solvents alter the bulk properties of the solvent differ-

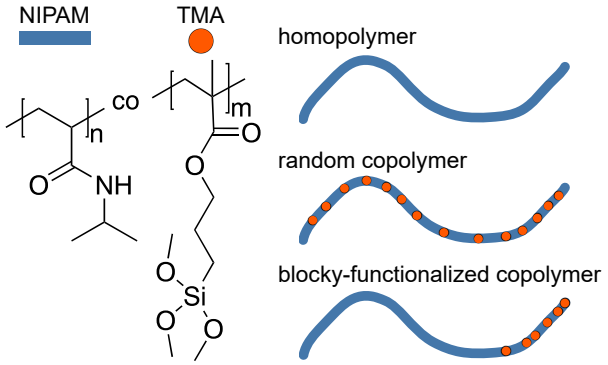

Fig. 1 Chemical structure of the polymer of P(NIPAM-*co*-TMA) and cartoon schematics of copolymer architectures of interest. The blue segments represent PNIPAM and the orange circles represent TMA repeat units. Throughout the manuscript, similar cartoons are used to demonstrate the architecture and relative block size for the investigated polymers, but the size of the TMA units is increased for visual clarity thus, is not to scale.

ently. For example, we show that for ethanol-containing systems, a TMA content and configuration dependent effect on aggregate structure size occurs; however, these polymer structure changes do not substantially alter the transition temperatures. In contrast, we demonstrate that DMF incorporation shows synergistic effects with TMA, leading to earlier onset transitions. Additionally, unique and thermoreversible optical responses are observed at certain DMF compositions. Overall, cosolvent species and content can be used to tune both the transition temperatures and the structure sizes of NIPAM/TMA copolymers – a strategy that enables a versatile range of covalently-crosslinked structures, such as particles and coatings, for applications including sensing, separations, and drug delivery.

2 Materials and methods

2.1 Materials

1-propanol ($\geq$ 99.5%, ACS grade), methanol ($\geq$ 99.8%, ACS grade), and molecular sieves (3 Å) were purchased from Sigma-Aldrich. *N,N*-dimethyl formamide (ACS grade) was purchased from Fisher Scientific. Anhydrous ethanol (200 proof) was purchased from Decon Labs, Inc. Organic solvents were dried over molecular sieves prior to use. Solvent-compatible UV cuvettes were purchased from Sarstedt.

2.2 Polymer synthesis

The polymers used in this work were synthesized as described in a previous report by Linn *et al.*[32] Detailed polymer characterization data is available in the supplementary information of that manuscript and in SI.1.1. Briefly, reversible addition-fragmentation chain transfer polymerization was used to synthesize polymers of controlled molecular weight and dispersity. Azobisisobutyronitrile was used as the initiator, 2-(ethylsulfanylthiocarbonylsulfanyl)-2-methylpropionic acid as the chain transfer agent, synthesis of which has been documented in several prior reports,[32,53,54] and 1,4-dioxane as the reaction solvent. For PNIPAM homopolymers and random copolymers of NIPAM and TMA, all reagents were added to the reaction flask prior to degassing via three freeze/pump/thaw cycles. For blocky-functionalized copolymers of NIPAM and TMA, a NIPAM homopolymerization was initiated, then after an intermediate conversion was reached, TMA was injected. Polymers were purified by repeated precipitation and dried under vacuum prior to analysis. Molecular weight and dispersity were characterized via size exclusion chromatography with multi-angle light scattering. Polymer purity and TMA incorporation were measured via ^{1}H-NMR spectroscopy in $CDCl_3$. Reactivity studies demonstrated that TMA and NIPAM incorporated approximately randomly across all monomer feedstock compositions, with a slight preferential incorporation of TMA.[32] The polymers investigated in this report are described in Table 1. This report focuses on polymers with relatively higher TMA contents that exhibit distinct behavior from PNIPAM homopolymers, as opposed to low TMA contents which behaved similarly to PNIPAM controls in prior studies.[32] All polymers in this report are of well-controlled dispersity ($Đ \leq 1.2$), with the exception of the copolymer with 10.1% mol TMA which has a higher dispersity due to the propensity for crosslinking during purification at high TMA contents (Figs. S1&S2).

Herein, polymers will be denoted as follows: N_x represents a poly(*N*-isopropyl acrylamide) homopolymer with a number-average degree of polymerization x; N_x/T_y represents a random poly(*N*-isopropyl acrylamide-*co*-3-(trimethoxysilyl)propyl methacrylate) copolymer with number average degrees of polymerization x and y of NIPAM and TMA, respectively; and, $N_x[N_y/T_z]$ represents a blocky-functionalized copolymer with with x NIPAM units in the homopolymer A-block, and y NIPAM and and z TMA units in the copolymer B-block. For clarity, Fig. 1 shows cartoons of the different polymer architectures investigated in this report, where the blue portions represent PNIPAM and the orange circles represent TMA units.

2.3 Dynamic light scattering (DLS)

Dynamic light scattering was conducted to assess the hydrodynamic diameter, D_h, of polymer chains and aggregates as a function of temperature and co-solvent quantity. Samples were prepared at fixed polymer content of 0.1% wt in the desired water/cosolvent system and filtered with a 0.2 μm PTFE syringe filter prior to analysis. Viscosity values and refractive indices of the solvent mixtures were either estimated based on literature values[55–58] (SI.1.2) or, in the case of low organic content ($\leq$ 5% mol), were constructed using the complex solvent builder in the Malvern Zetasizer software.

A standardized thermal control sequence was used to ensure that each sample had similar thermal history. A typical control sequence started at 20 °C with measurements taken at 5 °C increments. The sample was allowed to equilibrate for 3 minutes at each temperature prior to data collection. At each temperature, 8 measurements consisting of 5 runs of 5 s were collected. These measurements were then analyzed and averaged in the Malvern Zetasizer Software before analysis. A typical control sequence for these experiments covered a range of temperatures from 20 to 45 °C, as is shown in Fig. S6. The D_h at $T > T_{CP}$ referenced throughout this work was taken at the highest temperature and after the

Table 1 Table listing relevant parameters of the polymers investigated in this report.

Polymer	Abbreviation	M_n[a] (kDa)	$Đ$[a]	$F_{TMA,AB}$[b] (% mol)	$F_{TMA,B}$[a,b] (% mol)	$T_{CP,1}$[c] (°C)	$T_{Cl,1}$[c] (°C)
P(NIPAM$_{408}$)	N_{408}	46.2	1.13	0	–	34.0	31.2
P(NIPAM$_{479}$)	N_{479}	54.2	1.15	0	–	33.1	30.9
P(NIPAM$_{456}$-co-TMA$_2$)	N_{456}/T_2	52.1	1.11	0.5	–	33.1	30.7
P(NIPAM$_{400}$-co-TMA$_{14}$)	N_{400}/T_{14}	48.7	1.19	3.5	–	33.1	–
P(NIPAM$_{783}$-co-TMA$_{88}$)	N_{783}/T_{88}	110	2.43	10.1	–	32.6	–
P(NIPAM$_{293}$-b-NIPAM$_{143}$-co-TMA$_8$)	$N_{293}[N_{143}/T_8]$	50.3	1.10	1.9	5.2	32.8	27.3
P(NIPAM$_{283}$-b-NIPAM$_{113}$-co-TMA$_8$)	$N_{283}[N_{113}/T_8]$	46.8	1.10	2.0	6.6	33.6	31.6

[a]Determined via SEC-MALS. [b] Determined via ^{1}H NMR spectroscopy. [c]Determined via cloud point testing in aqueous solutions (λ = 405 nm).

D_h had reached a plateau value with temperature, typically 40 or 45 °C (an example of the plateau in D_h is shown in Fig. S6a).

2.4 Cloud point testing (CPT)

Cloud point measurements were conducted on an instrument developed in house,[54,59] and are performed in a manner similar to our prior work.[32] Samples were prepared at 1% wt polymer and filtered through a plug of glass wool prior to characterization. The cuvettes were then sealed with a commercial two-part epoxy and allowed to cure for approximately an hour before analysis. Sealing the cuvettes limited sample evaporation to less than ~0.5% of the original sample mass, even for experimental protocols up to 18 h. A violet laser (5 mW, 405 nm) was used to assess the transmittance of the sample. A ramp rate of 0.2 °C/min was used during the temperature ramps. Samples were equilibrated for at least 10 minutes at 25 °C, prior to a temperature ramp to 45 °C. This temperature was held constant for 5 minutes prior to a temperature ramp back down to 25 °C. For samples that were characterized over multiple thermal cycles, this thermal cycling procedure was repeated three more times, with a 5 minute hold at 25 °C between each cycle. The minimum temperature during each thermal cycle was adjusted lower as necessary at higher organic contents to capture the optical transition.

The raw transmittance values were normalized by dividing the transmittance by the maximum transmittance on the first thermal cycle. The cloud point temperature (T_{CP}) upon heating and clearing temperature (T_{Cl}) upon cooling were extracted by first taking a smoothed first derivative of the normalized transmittance. This derivative was then fit to a Lorentz peak to extract T_{CP}, T_{Cl}, and the transition width, w. An example of this fitting procedure is shown in Fig. S4.

3 Results and discussion

3.1 Screening structure size with solvent and temperature

Screening experiments across a range of solvent species and compositions were first performed to identify solution conditions that can dramatically alter the structures formed at high temperatures.

3.1.1 Thermally-induced structuring in aqueous systems

In aqueous systems, TMA incorporation into PNIPAM can dramatically alter the size and uniformity of the structures formed above the lower critical solution temperature phase boundary.[32] Here, an increase in TMA content reduces the aggregate structure size. Localization of the TMA to one chain end further decreases the structure size and leads to formation of uniform spherical micelles, validated by cryo-TEM.[32] Thus copolymers with 'blocky-localized' TMA display assembly behavior above T_{CP}, compared to the large and highly disperse aggregates formed by PNIPAM homopolymers and TMA-containing random copolymers. This structure uniformity corresponds to a narrower peak width and lower *PDI* at high temperatures in dynamic light scattering (DLS), confirmed by observations from cryo-TEM (Fig. S5).

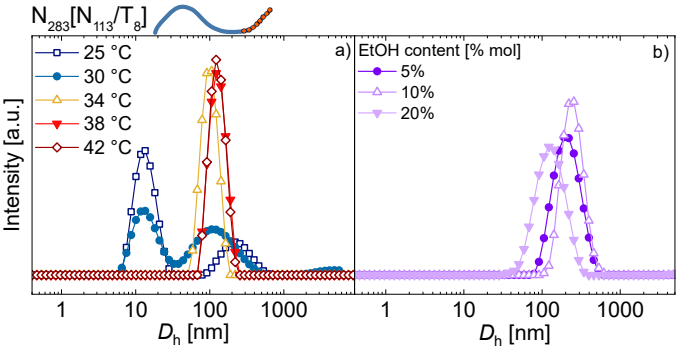

Fig. 2 Size distributions of blocky-functionalized polymer $N_{283}[N_{113}/T_8]$ via DLS in (a) water as a function of temperature, and (b) in increasing ethanol content at 25 °C. An increase in D_h is observed with both increasing temperature and organic content as polymer chains undergo a conformational collapse prior to micellar assembly and aggregate into larger structures.

The blocky-functionalized copolymer, $N_{283}[N_{113}/T_8]$, displays micellar assembly in aqueous conditions at temperatures above the LCST phase boundary. At low temperatures, bimodal populations are observed in aqueous $N_{283}[N_{113}/T_8]$ (Fig. 2a), where predominantly unimers are observed with a smaller population of larger hydrodynamic diameter (D_h) structures. These higher D_h structures suggest some association due to the TMA units, as this higher D_h peak at 25 °C is not observed in homopolymers (Fig. S7). As the temperature increases, the unimer peak decreases in intensity and the higher D_h peak decreases in size. Above T_{CP} a single uniform distribution is observed, with low PDI (D_h =121 ± 0.8 nm, *PDI* =0.035), which is substantially smaller and less disperse than a homopolymer control (N_{408}, D_h =277.4 ± 1.4 nm, *PDI* =0.12). These uniform micellar structures form at surprisingly low overall TMA content (~ 2% mol).

3.1.2 Structure formation at high cosolvent incorporation

The incorporation of organic cosolvents was used as a method to assess how robust this assembly of blocky-functionalized polymers is to environmental conditions. The two-phase region in which these structures form can be accessed by increasing temperature or incorporating cosolvent; to narrow the experimental parameter space, screening was first done at high cosolvent content (T = 25 °C) where solution composition changed dramati-

cally. While the changes in transition temperature with increasing solvent content are due to the co-nonsolvency effect, throughout this report the incorporated organic solvent is referred to as a cosolvent for clarity as the majority of the experiments are performed across the LCST phase boundary.

$N_{283}[N_{113}/T_8]$ does not exhibit uniform assembly in the two-phase co-nonsolvent region when screened at higher cosolvent content at 25 °C, as observed by DLS. Here, ethanol compositions between 5-20% mol are at or above the LCST, demonstrated by the average structure sizes above 100 nm for each of these solvent compositions (Fig. 2b). Similar to prior observations,[41,60] the transition temperature of PNIPAM decreases precipitously with increasing ethanol content in the water-rich regime (Fig. 3), such that at 5% mol EtOH at 25 °C, the polymer chains are collapsed and aggregated in a large and broad distribution (D_h =190 ± 5 nm, PDI =0.12). Increasing the ethanol content to 20% mol decreases the aggregate size (D_h =117 ± 3 nm), likely due to worsening solvent quality as this composition is further away from the single phase boundary. However, the structural polydispersity increases further (PDI =0.16), suggesting that the blocky-functionalized copolymer is not forming uniform micelles at this high EtOH content. Across the range of 5-20% mol ethanol, similar sizes and wide PDIs are observed (Fig. S9). Similar trends of large D_h and PDI are observed across aqueous methanol content (Fig. S10).

These findings suggest that assembly phenomenon observed in polymers with blocky-localized TMA is diminished by large amounts of amphiphilic cosolvent. Ethanol may more effectively solvate both PNIPAM homopolymer and TMA-containing blocks, as PNIPAM does not exhibit LCST behavior in pure ethanol.[41,61] Beyond the cosolvent effects, the thermal control sequence also likely plays a substantial role in the structures formed by the blocky-functionalized polymers. Therefore, the effect of crossing the phase boundary into the two-phase region by varying both the temperature and cosolvent content is of interest to assess how cosolvent incorporation alters the structure size and uniformity.

3.1.3 Structure formation at low cosolvent incorporation

Given that high cosolvent content eliminates assembly in blocky-functionalized copolymers, the effect of cosolvent species on aggregate structure above T_{CP} was next assessed at low cosolvent content in several cosolvent species. This screening of the assembly behavior was done using a standardized temperature sequence with DLS (Section 2.3, Fig. S6). Given the large structure size difference observed between aqueous homopolymer N_{408} and blocky-functionalized copolymer $N_{283}[N_{113}/T_8]$, the ratio between these structure sizes was used as a heuristic to assess the robustness of the micellar assembly in the blocky-functionalized polymer. This ratio is defined as $\frac{D_{h,HP}}{D_{h,BCP}}$, where $D_{h,HP}$ is the hydrodynamic diameter of the homopolymer and $D_{h,BCP}$ is the structure size of the blocky-functionalized copolymer; $\frac{D_{h,HP}}{D_{h,BCP}} = 3.2$ in aqueous systems. Of particular interest are systems where this ratio changes the most from that in water, suggesting that the cosolvent is altering the aggregation mechanism.

Across screening trials spanning eight solvent compositions (Fig. S8), the $\frac{D_{h,HP}}{D_{h,BCP}}$ ratio was largest in purely aqueous systems. Addition of low cosolvent amounts (≤5% mol), regardless of species and content, decreased this ratio. For example, methanol and 1-propanol incorporation modestly increased the structure sizes for the blocky-functionalized copolymer, but did not lead to as significant of a change in $\frac{D_{h,HP}}{D_{h,BCP}}$. Here, ethanol and *N,N*-dimethyl formamide were identified as the cosolvents that reduced the size ratio closest to unity in the water-rich regime – suggestive of significantly altered aggregation mechanisms.

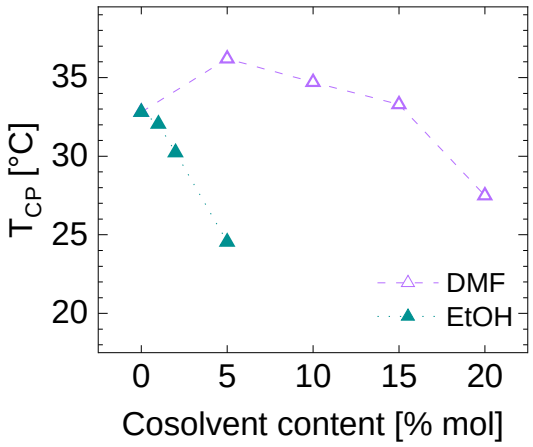

Fig. 3 Comparison of the LCST phase boundaries of N_{479} for EtOH and DMF across the compositions investigated in this report.

Interestingly, these two solvents appear to reduce $\frac{D_{h,HP}}{D_{h,BCP}}$ by different means. While ethanol reduces the structure size formed by the homopolymer to reduce $\frac{D_{h,HP}}{D_{h,BCP}}$, DMF instead substantially increases D_h for blocky-functionalized polymer (Fig. S8). EtOH and DMF systems are also interesting because the polymer/water/cosolvent phase diagrams share similar features (i.e. both exhibit a lower critical solution temperature boundary and an upper critical solution boundary), but these components interact differently in the bulk. For example, in these ternary systems, ethanol is considered kosmotropic, a structure former, where DMF is chaotropic, a structure breaker.[42,62,63] Further, while EtOH incorporation rapidly decreases T_{CP} below room temperature, substantially higher organic content can be reached in DMF-containing systems without suppressing T_{CP} below room temperature (Fig. 3). Thus, to better understand the unique mechanisms altering structure formation at elevated temperatures, ethanol and DMF were chosen as the co-solvents of interest for the remaining investigation, with ranges of organic content shown in Fig. 3 to keep a comparable range of T_{CP}.

3.2 Impact of ethanol on the thermoresponsiveness of P(NIPAM) and P(NIPAM-*co*-TMA)

3.2.1 Ethanol tunes structure size and assembly

Low incorporation of ethanol cosolvent dramatically alters the transition temperatures, optical behavior, and structure size above T_{CP} of aqueous PNIPAM homopolymer and P(NIPAM-*co*-TMA). These transmittance responses upon heating were probed between 0 to 5% mol EtOH in N_{479} (Fig. 4). As expected based on prior reports,[41,61] T_{CP} decreases as the ethanol content increases. Interestingly, at 2% mol EtOH, a substantially diminished

transmittance response is observed above T_{CP}, where a transmittance of ~0.6 is retained at elevated temperatures (Fig. 4a). This reduced transmittance drop has previously been attributed to a reduced aggregate size above T_{CP}.[32] However, this trend is non-monotonic, and the full transmittance drop at high T occurs again at and above 3.5% mol EtOH.

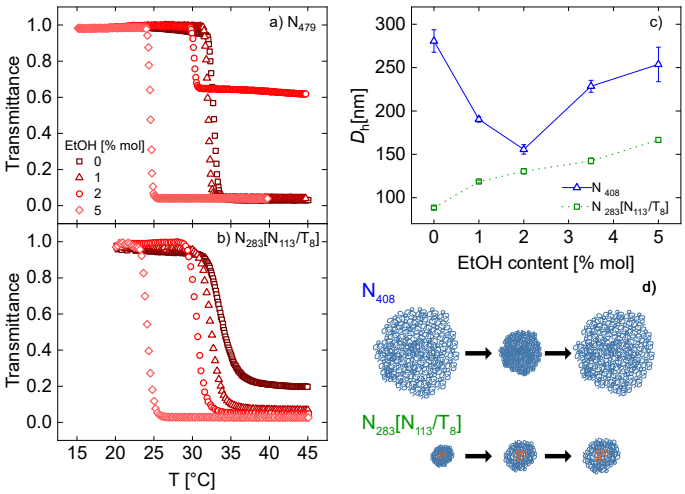

Fig. 4 Transmittance response of a) PNIPAM homopolymer N_{479} and b) blocky-functionalized copolymer $N_{283}[N_{113}/T_8]$ with varying ethanol content (0-5% mol). c) Hydrodynamic radii of structures formed above T_{CP} show different dependencies on ethanol content depending on polymer configuration (Fig. S11). d) illustration of relative structure sizes formed above T_{CP} with increasing ethanol content for N_{408} and $N_{283}[N_{113}/T_8]$.

In contrast, both T_{CP} and the minimum transmittance at high T monotonically decrease with increasing EtOH content for the blocky-functionalized $N_{283}[N_{113}/T_8]$ (Fig. 4b). Even 1% ethanol incorporation leads to a significant loss in transmittance in the blocky-functionalized copolymer. Despite the visually distinct optical transitions between the homopolymer and TMA blocky-functionalized copolymer (Fig. 4a-b), the cloud point temperatures, defined as the temperature of maximum slope (Fig. S4), are all within 0.5 °C between the two polymers at a given solvent composition. The impact of TMA content on the phase diagram in water/EtOH systems is discussed in more detail in Section 3.3.1.

To investigate the differences in the minimum optical transmittance at high temperatures between a homopolymer and block-functionalized polymer, dynamic light scattering was performed across the LCST phase transition to assess the D_h of the structures formed above T_{CP}. Prior work using direct imaging confirmed that this D_h above T_{CP} corresponds with the size of the structures that form.[32] While cloud point measurements were performed using homopolymer N_{479} to enable consistent comparison with DMF-containing cosolvent mixtures (Sec. 3.3.3), here homopolymer N_{408} was used for comparison of structure sizes due to its molecular weight similarity to $N_{283}[N_{113}/T_8]$. Notably, the homopolymers of different molecular weights used in Fig. 4a vs. 4c have similar D_h above T_{CP} in water.[32]

The hydrodynamic diameters of the structures formed with increasing ethanol content trend differently for N_{408} and $N_{283}[N_{113}/T_8]$ (Fig. 4c,d). The blocky-functionalized $N_{283}[N_{113}/T_8]$ shows a monotonic increase in aggregate size with increasing ethanol content – confirming that the monotonic decrease in minimum transmittance with increasing EtOH from cloud point testing is due to scattering from increasingly larger structures. In contrast, the homopolymer N_{408} has a local minimum in D_h at 2% mol ethanol (D_h = 156 ± 5 nm), again suggesting that the higher minimum transmittance at 2% mol EtOH in Fig. 4a is due to formation of smaller structures.

While both homopolymer and blocky-functionalized copolymer display a reduced T_{CP} due to the co-nonsolvent effects of ethanol incorporation in water, the ethanol alters the hydrodynamic diameter of structures formed at high T differently, likely due to mechanistic differences in how these structures form. The TMA localization clearly plays an important role in the formation of uniform micelles,[32] as copolymers with random TMA incorporation display behavior similar to PNIPAM homopolymers at low ethanol incorporation. Here, D_h substantially decreases for random copolymers in 2% mol EtOH vs. in water: for N_{456}/T_2, D_h decreases from 371 ± 4 nm in water to 167 ± 9 nm in 2% mol EtOH (Fig. S12) and for N_{400}/T_{14}, D_h decreases from 211 ± 4 nm to 149 ± 3 nm (Fig. S13). Here, N_{400}/T_{14} displays a smaller relative decrease in aggregate size above T_{CP} in ethanol-containing solutions compared to N_{408} and N_{456}/T_2; this behavior is likely because N_{400}/T_{14} already exhibits a more compact aggregate structure in water due to its high TMA content.[32]

Interestingly, the hydrodynamic diameters for N_{400}/T_{14} and homopolymer N_{408} are statistically identical at 2% mol EtOH. This similarity in structure size suggests that the power of randomly-distributed TMA groups to reduce the aggregate structure size above T_{CP} is significantly limited in ethanol-containing solvent mixtures. One possible explanation is that the amphiphilic nature of ethanol allows this cosolvent to better solvate the TMA group than water, thereby reducing the ability of randomly-distributed TMA groups to significantly alter the structure size.

The decreased structure size at 2% mol EtOH above T_{CP} in the homopolymer and randomly-functionalized P(NIPAM-*co*-TMA) may be attributed to a decrease in the solvent-excluded volume contribution to the free energy of the polymer collapse, which is at a minimum at low EtOH incorporation (~2.5% mol).[64] This minimum occurs at the cosolvent concentration where the globule surface is saturated with cosolvent. This cosolvent saturation at the surface may hinder structure growth by interrupting aggregation, leading to smaller structures. Polymers that form larger structures in aqueous solutions must undergo more aggregation events in comparison to polymers that form small structures in aqueous systems. Thus, polymers that have a smaller structure size may experience a smaller reduction in D_h at low ethanol incorporation, as in the case of N_{400}/T_{14}.

In contrast to homopolymers and random copolymers, $N_{283}[N_{113}/T_8]$ has a monotonic increase in D_h with increasing ethanol content in the range of 0-5% mol. While the hydrodynamic diameters of N_{408} and $N_{283}[N_{113}/T_8]$ are similar at 2% mol EtOH (within ~20%), the structure size for the blocky-functionalized polymer remains smaller across this EtOH range (Fig. 4c). Instead, greater incorporation of the amphiphilic ethanol leads to gradual increases in D_h up to 5% mol, which

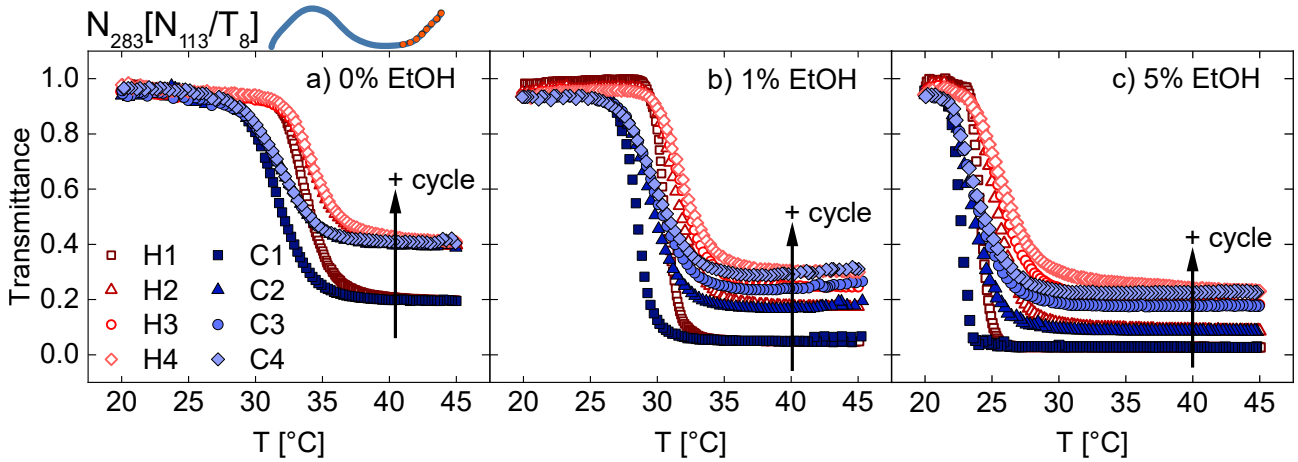

Fig. 5 Optical response over several thermal cycles $N_{283}[N_{113}/T_8]$ in solvent systems with a) 0% mol, b) 1% mol, and c) 5% mol ethanol. Ethanol incorporation leads to a decrease in minimum transmittance at high and the transmittance responses upon thermal cycling do not overlap as closely as in aqueous systems.

may be due to the cosolvent swelling the aggregate structures or an increase in the aggregation number of the structures. These trends in D_h across low EtOH contents for a PNIPAM homopolymer and $N_{283}[N_{113}/T_8]$ are illustrated in Fig. 4d.

Across the range of 0-5% mol ethanol, substantially larger changes in aggregate size are observed in the homopolymer (Fig. 4c), where a two-fold decrease occurs between 0 and 2% mol EtOH. Blocky-functionalized $N_{283}[N_{113}/T_8]$ exhibits a smaller total change in structure size, with a roughly 50% increase in D_h over the entire range of 0-5% mol EtOH. Although the structure size is increasing, assembly-like structuring is likely occurring, as the *PDI* values are low ($\leq$0.07) and are on average lower than the *PDI* values for N_{408} (Fig. S14). In agreement with prior work,[32] the homopolymer displays the smallest transmittance drop when the smallest structure sizes are present (2% mol EtOH), but a full transmittance drop at other solvent compositions where larger structures form. These trends in structure size with EtOH content qualitatively correspond with the CPT results for both polymers (Figs. 4a, c). Note that the relationship between minimum transmittance at high T and hydrodynamic diameter can only be compared for an individual polymer species, as the differences in the aggregate distributions, and thus the population of light scattering structures, lead to distinct transmittance responses.

3.2.2 Ethanol impact on thermoreversibility of blocky-functionalized copolymers

Blocky-functionalized polymers display good thermoreversibility in purely aqueous systems[32]; however, $N_{283}[N_{113}/T_8]$ displays two distinct transmittance responses depending on how many times the system has been thermally cycled (Fig. 5a). The greatest transmittance response is observed on the first cycle, then subsequent cycling leads to a decreased magnitude of transmittance response, which overlap closely. The high cyclability observed in these blocky-functionalized copolymers vs. analogous random-functionalized copolymers was previously attributed to the large domains of PNIPAM homopolymer in the non-functionalized block. The presence of these homopolymer domains was proposed to limit the extent of permanent crosslinking between silane groups that occurs in the structures that form above T_{CP}, improving thermoreversibility relative to the random copolymers.[32] Thus, these small structures are lightly crosslinked after the initial heating, leading to a decreased and broadened optical response with additional cycling. Additionally, there is assembly-like behavior where the TMA interacted preferentially with other TMA-containing blocks due to differences in hydrophilicity compared to PNIPAM. Ethanol incorporation may slightly disrupt this assembly-type structure formation leading to larger structure sizes, as the ethanol may more effectively solvate the TMA units than water due to its amphiphilicity.

Despite ethanol disrupting the assembly-like behavior in the blocky-functionalized polymers, evidence of the micellar assembly is still present up to 5% mol EtOH, both based on the reduced D_h vs. the homopolymer and in the behavior upon thermal cycling. These blocky-functionalized polymers display distinct transmittance responses over multiple thermal cycles, as seen in Fig. 5, which shows the transmittance of $N_{283}[N_{113}/T_8]$ with increasing ethanol content in the range of 0 to 5% mol EtOH. Each plot shows four subsequent heating and cooling cycles over the range of 20 to 45 °C, where the transmittance upon heating is shown in shades of red and cooling in blue. Even at 1% mol incorporation of EtOH, deviation from the behavior in the purely aqueous system is observed (Fig. 5b). In particular, the aqueous system displayed only two distinct transmittance responses, with the optical response stabilizing upon repeated cycling after the second cycle. Conversely, the minimum transmittance upon repeated cycling gradually increases with increasing cycle number for the 1% ethanol-containing system (Fig. 5b). This increase in transmittance at $T > T_{CP}$ corresponds to a relative decrease in structure size with repeated thermal cycling (Figs. S18, S19). Thus, compared to the aqueous system, the transmittance response does not overlap as closely upon repeated cycling; however, a large optical response is still observed upon repeated cycling, indicating a high degree of thermoreversibility.

Similar behavior upon cycling is observed at 5% mol EtOH, where the transition is clearly shifted to lower temperatures and the minimum transmittance increases slightly with each thermal

cycle (Fig. 5c). Once again, the optical response does not stabilize after two cycles suggesting that ethanol incorporation disrupts the mechanism of uniform structure formation observed in $N_{283}[N_{113}/T_8]$. However, ethanol incorporation up to 5% mol does not completely disrupt this mechanism, as additionally evidenced by the trends in the critical temperatures and transition widths, w (Figs. S20, S21). While ethanol incorporation shifts T_{CP} and w, these values are lowest during the first thermal cycle and then increase and plateau upon additional cycling – a characteristic trend of the structure formation in aqueous blocky-functionalized P(NIPAM-*co*-TMA).[32]

For water/ethanol mixtures in the water-rich regime, Tavagnacco *et al.*[65] report that the number of ethanol molecules in the first hydration shell around PNIPAM is greater than that in the bulk solution above the transition temperature; similar findings of cosolvent localization have been reported by numerous others.[64,66] Thus, one potential explanation for the behavior with increasing ethanol content in $N_{283}[N_{113}/T_8]$ is that solvent localization of ethanol with PNIPAM at elevated temperatures could disrupt the preferential interactions in the TMA-containing blocks that contribute to the assembly behavior at high T. Here, the amphiphilic character of ethanol can better solvate the TMA units, leading to a gradual increase in structure size and lower transmittance at high temperatures with increasing EtOH content.

The non-overlapping transmittance responses on cycles 2-4 in systems with alcohol suggest that additional structural changes are occurring with each cycle; this hypothesis is supported by DLS measurements after two cycles and at long times (Figs. S18, S19). In the aqueous case, the ordered structure limits the crosslinking after the first cycle, leading to closely overlapping transmittance responses. In contrast, in ethanol-containing systems, the cosolvent disrupts the preferential interactions of the TMA-containing blocks, reducing the TMA coupling that occurs during each thermal cycle. One possible explanation for the reduced TMA coupling is that ethanol incorporation may reduce methoxysilane hydrolysis by shifting the equilibrium towards the non-hydrolyzed silanes. Additionally, ethanol could form ethoxysilane groups, which hydrolyze more slowly than methoxysilanes.[67] As hydrolysis must occur prior to silane condensation, ethanol incorporation could reduce the crosslinking occurring in each thermal cycle, leading to the observed non-overlapping transmittance responses. Thus, with each thermal cycle, the TMA can continue to couple, leading to more compact structures with a decreased, but still substantial transmittance response. Across the range of ethanol compositions, the minimum transmittance above T_{CP} increases with thermal cycling for $N_{283}[N_{113}/T_8]$, as seen in Fig. 5b-c. This trend in minimum transmittance with each cycle suggests that additional thermal treatment may be necessary for blocky-functionalized copolymers to achieve structures with consistent transmittance responses in ethanol-containing systems, as the transmittance differences between each thermal cycle decrease with increasing cycle number.

While ethanol incorporation weakens some assembly effects in blocky-functionalized copolymers, the cosolvent does not negatively impact thermal cyclability. With each thermal cycle shown in Fig. 5 the differences between adjacent cycles decrease, suggesting that further heating and cooling would likely lead to closely overlapping responses. Compared to the purely aqueous system, ethanol-containing systems actually display a more significant transmittance loss on repeated cycling. While cosolvent leads to more variation in thermal responses, higher ethanol contents lead to a larger transmittance drop, which may be advantageous in certain applications where a large signal is required, such as sensing.

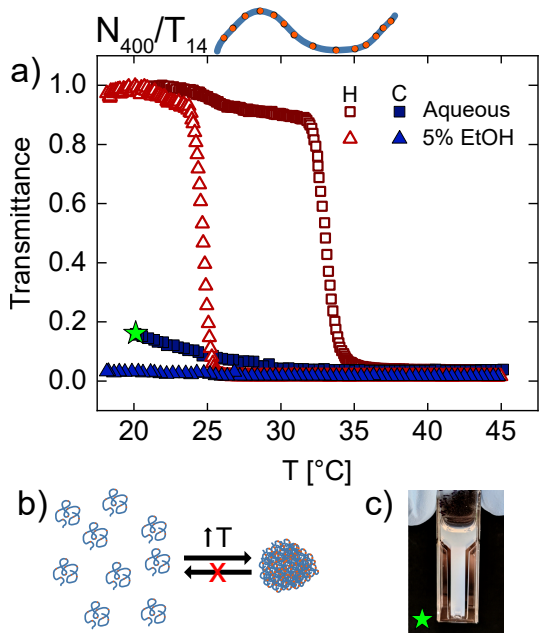

Fig. 6 a) Optical responses of N_{400}/T_{14} during the first heating and cooling cycle in water (squares, $T_{CP,1} = 33.1$ °C) and in 5% EtOH (triangles, $T_{CP,1} = 24.7$ °C) display very limited recovery after heating, where cosolvent incorporation primarily adjusts $T_{CP,1}$; b) cartoon illustrating that the aggregation and crosslinking of the random copolymer is not thermally reversible; c) sample after thermal cycling at room temperature displays significant irrecoverable opacity.

Interestingly, ethanol incorporation does not uniformly increase optical responses upon cycling for NIPAM/TMA copolymers. For example, the random copolymer N_{400}/T_{14} displays almost no transmittance recovery in 5% mol EtOH (Fig. 6a), whereas the analogous system in water recovers ~20% transmittance upon cooling. This nearly-zero recovery occurs because the aggregate structures that form above T_{CP} do not break up at low temperatures (Fig. 6b) – a feature previously attributed to silane crosslinking that occurs at elevated temperatures.[32,68] DLS experiments support this explanation, as the structure size formed at high temperatures is preserved upon cooling (SI.2.3). These large crosslinked structures lead to irreversible optical cloudiness (Fig. 6c). The lower transmittance recovery for N_{400}/T_{14} in 5% mol EtOH may be due to the ~10 °C lower cloud point temperature at this solvent composition: as the structure remains compact for significantly longer times at elevated temperatures, more silane crosslinking can occur.

3.3 Effects of TMA incorporation on phase boundaries in ethanol and DMF-containing systems

3.3.1 Polymer/water/EtOH phase boundaries are impacted minimally by TMA incorporation

Ethanol incorporation tunes the transition temperatures, structure size, and the optical response of PNIPAM homopolymers and TMA-containing copolymers, where the polymer architecture strongly influences the behavior (Sections 3.2.1 and 3.2.2). Notably, the observed differences in behavior resulting from the different architectures of the polymers are not simply the result of TMA incorporation leading to different phase boundaries. In fact, these phase boundaries in the water-rich regime are nearly identical across the systems explored – both here (Fig. 7a) and from prior work.[41] Specifically, the cloud point transition temperatures closely overlay up to 5% mol EtOH for a PNIPAM homopolymer (N_{479}), a random P(NIPAM-*co*-TMA) copolymer (N_{400}/T_{14}), a blocky-functionalized copolymer ($N_{283}[N_{113}/T_8]$), and a PNIPAM homopolymer previously reported by Costa and Freitas.[41] The close correspondence of the cloud point temperatures regardless of TMA content and configuration suggests that TMA addition is not an effective way to alter T_{CP} of PNIPAM-containing polymers at these solvent compositions. However, given the unique optical responses and structure sizes (Fig. 4), the similarity in transition temperatures *does* suggest that the solvent effects on the structure formation are decoupled from the initial conformational collapse. Instead, the changes in the thermal response with ethanol incorporation likely occur as the collapsed polymers aggregate, leading to different structure sizes and thus optical responses.

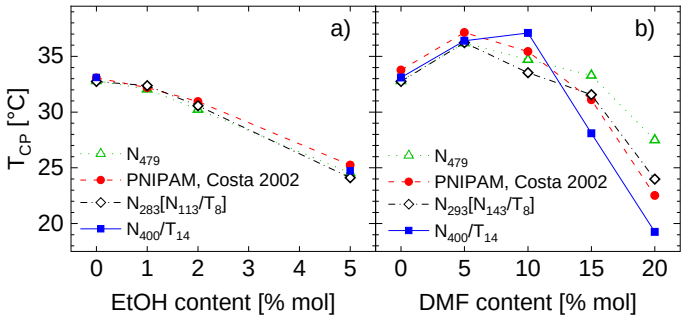

Fig. 7 Phase diagram of the LCST boundary of: a) polymer/water/EtOH solutions, and b) polymer/water/DMF solutions.

3.3.2 Changes in phase boundaries for EtOH vs. DMF-containing systems

N,N-dimethyl formamide (DMF) is an interesting comparison to EtOH, as the cosolvent composition range required to achieve a $\frac{D_{h,HP}}{D_{h,BCP}}$ ratio near unity is similar to that for ethanol ($\leq$5% mol). This ratio reduction (vs. in aqueous solution) occurs primarily due to a substantial increase in D_h above T_{CP} for the blocky-functionalized polymer (Fig. S8). At 5% mol DMF, both a homopolymer and blocky-functionalized copolymer of similar M_n exhibit a large size and broad *PDI* (Fig. S15). This similarity suggests that polymer-solvent interactions – rather than the polymer architecture – primarily control the structure size in systems with $\geq$5% mol DMF, and that the assembly of blocky-functionalized copolymers is disrupted at high DMF content.

Despite the structure size similarity between the homopolymer and blocky-functionalized copolymer, resulting LCST phase boundaries significantly differ at higher DMF contents depending on TMA content. In general, DMF in PNIPAM/water systems is considered to be a chaotropic agent,[41,42,69] or structure breaker; however, at low concentrations, DMF preferentially interacts with the polymer chains to effectively stabilize the hydrated polymer conformation.[28,41] This change in behavior results in a non-monotonic T_{CP} in the water-rich portion of the polymer/water/DMF phase diagram (Fig. 7b). Here, a local maximum in T_{CP} is observed in the range of 5-10% mol DMF depending on the specific polymer. Note that the slight discrepancies between the homopolymer control N_{479} and the data reported by Costa and Freitas[41] may arise due to a difference in the temperature ramp rate, which can systematically shift T_{CP}.[70]

Compared to aqueous systems containing ethanol, a greater than four-fold higher DMF content is required to reduce T_{CP} to a value near room temperature for the homopolymer N_{479}. Although T_{CP} depends on the specific polymer for high DMF contents (Fig. 7b), all polymer architectures require a several-fold increase in DMF content (relative to EtOH content) to observe the same changes in T_{CP}. To account for these differences, a wider range of DMF contents was explored here ($\leq$20% mol).

3.3.3 TMA incorporation in PNIPAM alters phase boundaries in aqueous *N,N*-dimethyl formamide

In contrast to the nearly-constant phase boundaries observed between polymers in ethanol-containing systems, TMA incorporation into PNIPAM-containing polymers leads to a decrease in cloud point transition temperatures at high DMF content (Fig. 7b). While the experimental cloud point temperatures for PNIPAM homopolymers and TMA-containing copolymers align closely at 0% and 5% mol DMF, at higher DMF concentrations, the behaviors diverge. The random copolymer N_{400}/T_{14} displays the most unique transition behavior with DMF composition, likely due to its relatively high TMA fraction (3.5% mol). While the other polymers exhibit a maximum T_{CP} near 5% mol DMF, the maximum T_{CP} for N_{400}/T_{14} is at $\sim$10% mol DMF – above which the T_{CP} values rapidly decline (Fig. 7b). While T_{CP} for N_{400}/T_{14} exceeds that of the other polymers at 10% mol DMF, T_{CP} values for N_{400}/T_{14} drop to values far below those of the homopolymer at $\geq$15% mol DMF.

By 20% mol DMF, an over 8 °C difference in T_{CP} is observed between the homopolymer and N_{400}/T_{14} copolymer, suggesting that T_{CP} more strongly depends on TMA content at higher DMF compositions. To test this hypothesis, the cloud point temperatures of polymers containing 0-10% mol TMA were examined as a function of DMF and TMA content (Fig. 8). At 0% DMF, the T_{CP} did not change much with TMA content; whereas, at elevated DMF contents, the cloud point temperatures decreased as a function of TMA content (Fig. 8a). Extracting slopes from these linear fits of T_{CP} vs. TMA content shows that these slopes increase in magnitude with increasing DMF content (Fig. 8b). This analysis reveals that an increase in the polymer TMA content leads to a greater decrease in T_{CP} at higher DMF contents. Unsurprisingly,

the blocky-functionalized copolymer $N_{293}[N_{143}/T_8]$ shows close alignment with the homopolymer control at DMF compositions <10% mol; however the T_{CP} above 10% mol DMF is intermediate between N_{479} and N_{400}/T_{14} – further suggesting that the effect may largely be controlled by the polymer TMA content.

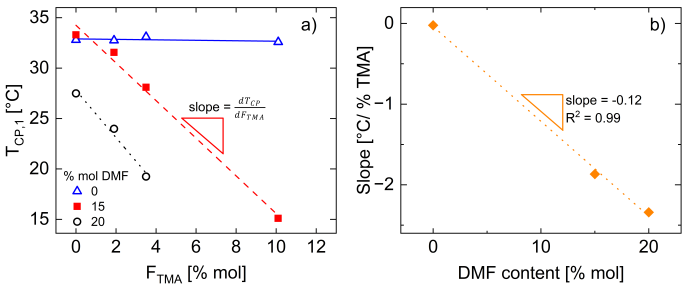

Fig. 8 a) Cloud point temperatures as a function of TMA content in the polymer at 0, 15, and 20% mol DMF. This range was selected where DMF acts as a structure breaker, leading to a decrease in T_{CP}. Linear fits of each trend are extracted and shown in b) as a function of DMF content. At high DMF compositions, the TMA incorporation and DMF content act synergistically to reduce T_{CP}.

The substantial decrease in T_{CP} with low TMA incorporation suggests that there are synergistic effects between the DMF and TMA causing the polymer chains to collapse and aggregate at lower temperatures. Substantial shifts in cosolvent systems with low degrees of comonomer incorporation have been reported previously. Zhang *et al.* [71] substantially altered the UCST phase boundary of poly(methyl methacrylate) (PMMA) in water/ethanol mixtures by substituting 4-8% mol of the PMMA units with a range of acrylamides. In that work, differences in the polarity and hydrogen bonding character of the acrylamide units led to substantial changes in the phase transition temperatures. While these PMMA systems are not directly equivalent to the P(NIPAM-*co*-TMA) systems presented here, especially considering that Zhang *et al.* [71] characterized the upper critical solution temperature in the cosolvent-rich portion of phase diagram, their report establishes that cosolvent phase boundaries can be altered with a few percent of a comonomer – and that the differences may be greater than in singular solvents.

The differences in how T_{CP} depends on F_{TMA} based on solvent composition may partially be attributed to the decreased hydrogen bonding between polymer and solvent. In pure water, a small negative slope is observed with increasing F_{TMA}. While both NIPAM and TMA repeat units have oxygens that can accept hydrogen bonds from water, NIPAM can also act as a hydrogen bond donor – thus one H-bond donor site is lost for each TMA monomer that replaces a NIPAM monomer. However, TMA has multiple oxygens that can accept H-bonds and water is both a hydrogen bond donor and acceptor. As such, the loss of the H-bond donor site may be offset by increased H-bonding at acceptor sites. As a result, little change in T_{CP} is observed with increasing F_{TMA} at 0% DMF. At 15% and 20% mol DMF, T_{CP} scales much more strongly with F_{TMA}; these DMF contents contain more than 50% DMF by volume. Unlike water, DMF can only accept hydrogen bonds – thus NIPAM can form H-bonds with DMF whereas TMA cannot. Therefore, as the TMA content increases – and the water content decreases – opportunities for the polymer to be well-solvated decrease. Accordingly, fewer H-bonds must be broken to access the two-phase region, leading to earlier onset chain collapse.

The linearity of the fit shown in Fig. 8b supports the hypothesis that the reduction in T_{CP} is controlled by a direct decrease in cosolvent/polymer interactions in the region where DMF incorporation decreases the transition temperature. However, hydrogen bonding differences alone likely do not explain the synergistic effect between TMA and DMF to lower T_{CP}, as the trend in T_{CP} with respect to TMA content does not hold at intermediate DMF contents where DMF acts as a structure former rather than structure breaker (Fig. 7b). Accordingly, the structure of the bulk solvent likely also plays a role; for example, above 13.5% mol DMF in water, the tetrahedral structure of water is disrupted, instead forming stoichiometric water/DMF complexes.[72] Hydrophobic hydration is thought to critically impact the PNIPAM aggregation process[42,73]; thus at these higher DMF contents, the ability of water to hydrophobically hydrate the polymer is likely diminished. The added bulkiness and hydrophobicity of the TMA group may also require additional solvent molecules to become well-hydrated.[74] Thus a combination of these effects likely leads to the strong synergistic effect of TMA and DMF content decreasing T_{CP}. This behavior in DMF starkly contrasts the EtOH-containing system, where the TMA content did not adjust the phase boundaries over a cosolvent ranges that decreased T_{CP} to a similar extent (Fig. 3).

3.4 Impact of *N,N*-dimethyl formamide (DMF) on the thermoresponsiveness of PNIPAM-containing polymers

3.4.1 Optical response of P(NIPAM-*co*-TMA) in aqueous DMF

PNIPAM homopolymer N_{479} displays similar transmittance responses across the range of 0 to 15% mol DMF; here, the DMF content adjusts where the phase transition occurs, and each composition demonstrates a full loss of transmittance with similar transition widths, w, in the range of 0.4-1 °C (Fig. S22). At 20% DMF, the transmittance response is substantially broadened (w = 2.2 °C) and the lowest transition temperature is observed (T_{CP} = 27.5 °C). This broadening may occur due to the substantially altered structure of the bulk solvent compared to lower DMF contents, as at this composition, the tetrahedral structure of water is destroyed, and the solvents form water/DMF complexes.[72] Additionally, DMF is the primary component by volume at 20% mol. These factors may lead to altered aggregation kinetics, leading to a broadening of the optical transition. In contrast to the aqueous ethanol systems (Fig. 4a), homopolymer N_{479} exhibits a full transmittance loss for all measured DMF compositions (Fig. S23). These transmittance responses suggest that the aggregate size remains quite large with increasing DMF content, unlike the trend observed in ethanol-containing systems.

Similarly to the homopolymer, DMF incorporation significantly alters the transition temperature for the random copolymer N_{400}/T_{14}. The optical responses of random copolymer N_{400}/T_{14} during the first heating cycle demonstrate a full loss of transmittance at 0, 5, 10, and 20% mol DMF (Fig. 9a). Systems containing 5% and 10% mol DMF demonstrate an increased T_{CP} compared to the purely aqueous system, as expected based on the phase

diagram in Fig. 7b. The cloud point temperature then sharply declines at 20% mol DMF. Up to 10% mol DMF, the optical transitions are substantially wider for N_{400}/T_{14} vs. the homopolymer despite nearly identical T_{CP}; this difference grows with increasing DMF content (Fig. S22). Interestingly, the transition widths are identical for both polymers at 15% mol DMF and above, despite their drastically different T_{CP} at these DMF compositions.

Note that only the first heating cycle is shown in Fig. 9a, as little transmittance recovery is observed upon cooling at these solvent compositions (Fig. S24). Similar to the N_{400}/T_{14} in water/ethanol, this loss of transmittance recovery is due to the aggregates crosslinking at high temperatures, which leads to permanent structures that cannot break up into unimers below the transition temperature (SI.2.3). The size of the crosslinked aggregates formed with DMF incorporation remain upon cooling to room temperature, and correspond with the structure sizes observed during screening using a different thermal protocol (Section 3.1.3). These results suggest that the aggregate size in water/DMF systems is relatively independent of thermal history, and demonstrate that different-sized crosslinked structures can be accessed by the same precursor polymer just by varying the solvent composition (SI.2.3).

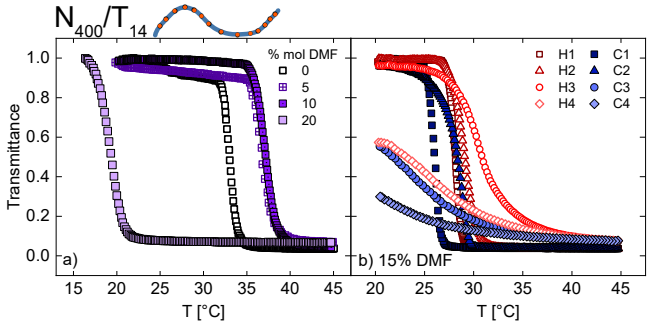

Fig. 9 a) Optical response during the first heating cycle of N_{400}/T_{14} at 0, 5, 10, and 20% mol DMF, where the DMF primarily alters T_{CP} during the first heating cycle (optical responses over four thermal cycles shown in Fig. S24), b) optical response of N_{400}/T_{14} at 15% mol DMF over four thermal cycles shows unique response with high cyclability.

Interestingly, a divergent behavior is observed upon thermal cycling for N_{400}/T_{14} in 15% mol DMF (Fig. 9b), where substantial transmittance recovery is observed for some cycles. Here, the first two cycles display full transmittance responses and recovery, whereas cycles three and four show gradual decreases in transmittance at low temperatures (Fig. 9b). This 15% mol DMF solvent appears to be a unique solvent composition, as systems with both higher and lower cosolvent incorporation do not display this response (Fig. S24). These systems instead display responses similar to one another and similar to the aqueous system, with little optical recovery after the first heating/cooling cycle due to silane crosslinking.

The optical response over several thermal cycles of the blocky-functionalized copolymer $N_{293}[N_{143}/T_8]$ is also highly dependent on the DMF content (Fig. 10). At 5% DMF (Fig. 10a), similar behavior is observed in DMF as in the ethanol systems (Fig. 5). Here repeated cycles do not overlap, and the minimum transmittance decreases with increasing cosolvent content. At 10% DMF, a full decrease in transmittance is observed in each thermal cycle (Fig. 10b). While T_{CP} increases with cycle number for both 5% and 10% mol DMF by ~1 °C (Fig. S25), the width of the optical transition greatly differs between the two solvent compositions. At 5% mol DMF, the transition widths increase dramatically after the first cycle, with a maximum $w \approx 7$ °C. In contrast, at 10% mol DMF, the transition widths remain in a much narrower range near 1 °C for all thermal cycles (Fig. S26).

At 15% mol DMF (Fig. 10c), a unique transmittance response is observed, similar to that observed for the random copolymer (Fig. 9c). Interestingly, the trends in the optical response of the blocky-functionalized copolymer are non-monotonic, where the third heating and cooling cycle has a decreased transmittance compared to the fourth cycle. This non-monotonic behavior does not occur at 15% mol DMF in N_{400}/T_{14}, as the transmittance response gradually decreases with repeated cycling, likely corresponding to additional crosslinking. However in the blocky-functionalized copolymer, crosslinking can only occur over a small portion of the chain, such that a large portion of PNIPAM must remain unconstrained even over many cycles. As such, these polymers retain a significant optical response over many cycles, even though the micellar assembly is not strong enough to alter the initial structure size (relative to the homopolymer).

Increasing the DMF content to 20% mol (Fig. 10d), a highly cyclable optical response is observed. However, an inversion of the trend in T_{CP} occurs, where the first thermal cycle has the highest transition temperatures and T_{CP} gradually decreases with increasing cycle number (Fig. S25). In thermoreversible aqueous systems[32] and cosolvent systems at lower organic fraction, the first thermal cycle typically has the lowest transition temperatures and repeated cycles display an increase in transition temperature (Figs. S20, S25). This inversion of the critical temperatures with thermal cycling suggests a substantially altered aggregate structure in systems with greater organic cosolvent, leading to earlier-onset optical clouding.

Interestingly, the divergent behavior with thermal cycling is observed at 15% mol DMF in both TMA-containing systems (Figs. 9b, 10c). This composition is likely near several key transitions in the behavior of the system, related to both the solvent/polymer interactions, and structural changes in the bulk solvent. Computational work performed by Zhu and Chen[69] suggests that when $T > T_{CP}$, PNIPAM interacts with the same number of water and DMF molecules at approximately 15% mol DMF. At higher organic content, the polymer interacts with a greater number of DMF molecules, and vice versa at lower DMF content. Thus, at compositions near this transition, the polymer chains may be experiencing non-equilibrium solvent interactions. Additionally, spectroscopic investigations by Yang *et al.*[72] show substantial changes in the water structure at 40% vol DMF (equivalent to 13.5% mol DMF). At this point, substantial quantities of DMF have been added to disrupt the tetrahedral structure of water, leading to the formation of water/DMF complexes.

While these structural transitions in the bulk solvent have minimal effect on the optical response of PNIPAM homopolymer (Fig. S23), the impact is substantial in TMA-containing polymers, suggesting that the nature and rate of the silane crosslinking reactions could be affected. Tokuyama *et al.*[45] reported the synthesis

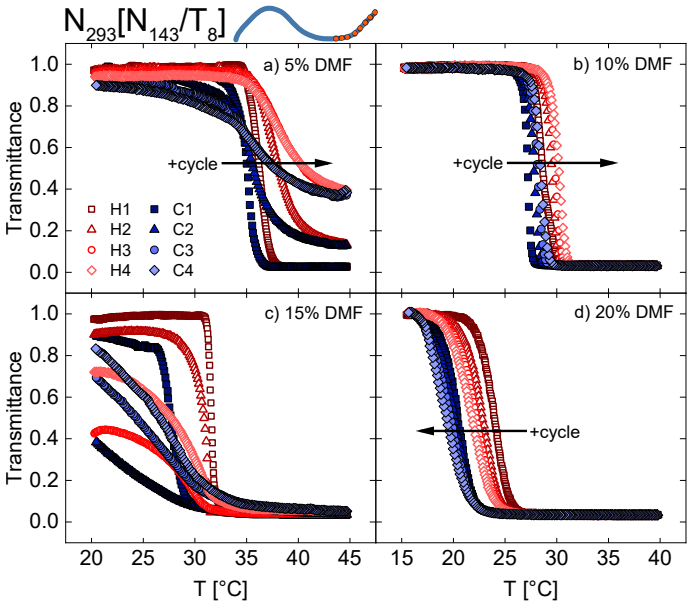

Fig. 10 Optical responses $N_{293}[N_{143}/T_8]$ in a) 5% mol, b) 10% mol, c) 15% mol, and d) 20% mol DMF compositions. Divergent, non-monotonic behavior is observed at 15% mol DMF in panel c.

of crosslinked, PNIPAM-containing gels in varying water/DMF ratios. Here, a morphological transition from a homogeneous to a heterogeneous, porous gel was observed at DMF compositions near 15% mol. The authors attribute this morphology change to the polymerizing network being excluded from the water/DMF clusters, thus occurring primarily in water-rich domains, leading to a highly porous structure. Additionally, a reduction in gelation kinetics was also observed in systems that formed this heterogeneous structure. A heterogeneous aggregate structure and slowed kinetics near 15% mol DMF may explain the increased cyclability of N_{400}/T_{14} (Fig. 9c) compared to other compositions, as the favorability of crosslinking above T_{CP} is decreased. Additionally, the non-monotonic behavior with thermal cycling that occurs in $N_{293}[N_{143}/T_8]$ (Fig. 10c) may result from the competing influences of the assembly-like behavior of the blocky-functionalized polymers and the heterogeneous solvent environment, leading to an unpredictable optical response.

3.5 Effects of cosolvent species on the thermoresponsive behavior of P(NIPAM-*co*-TMA)

The phase diagrams of ternary PNIPAM/water/EtOH and PNIPAM/water/DMF may appear similar, having both LCST and UCST phase boundaries;[41] however, the cosolvent species plays a key role in the response of various PNIPAM-containing polymers in the two-phase region. Low ethanol content primarily adjusts the size of the aggregate structures formed above the cloud point temperature. The effect of ethanol incorporation depends on TMA content and localization: PNIPAM homopolymers and P(NIPAM-*co*-TMA) copolymers with random TMA incorporation experience a minimum in structure size at 2% EtOH, whereas polymers with localized TMA demonstrate a monotonic increase in hydrodynamic diameter with increasing ethanol content. While randomly-incorporated TMA reduces structure sizes substantially in aqueous solutions,[32] random TMA incorporation has far less impact on structure size once ethanol is introduced as a cosolvent – leading to similar structure sizes as the homopolymer controls. However, similar to aqueous solutions, localized TMA incorporation has a far greater power to reduce the structure size than random TMA incorporation – an effect that lessens as EtOH content increases. Thus although these trends suggest that EtOH better solvates TMA thereby reducing its ability to control the structure size, sufficient quantities of localized TMA still cause assembly-like behavior in blocky-functionalized polymers.

These changes in structure size across polymer systems in water/EtOH are reflected in the transmittance responses of the polymers in cloud point measurements. Here, smaller structures lead to a decreased transmittance response, i.e. a full loss of transmittance is not observed. While EtOH does localize at the polymer compared to the bulk, which may lead to the observed structure size differences between polymer configurations, this localization does not cause significant changes in T_{CP} with varying TMA content. The conformational collapse of PNIPAM in water-ethanol mixtures is more strongly attributed to changes in the energetics of the bulk solvent,[42,65] which are likely not strongly affected by the presence of TMA in the polymer.

In contrast to EtOH-containing systems, systems containing DMF and TMA demonstrate synergistic effects, leading to more significant decreases in cloud point temperatures when both the TMA and DMF content are high. This behavior suggests that the reduction of hydrogen bonding between the cosolvent and polymer with increasing TMA is a controlling factor in when the conformational collapse occurs. Additionally, DMF incorporation allows the optical and phase transition to occur at experimentally accessible and biologically relevant temperatures – over a much wider composition range. These higher organic contents lead to unique behavior in the optical responses of P(NIPAM-*co*-TMA), which likely correspond to changes in both polymer/solvent interactions and structural changes in the bulk solvent, especially near 15% mol DMF.[69,72] The competing effects in polymer/water/DMF systems that lead to the observed phase behavior are highly complex, as evidenced by dramatic changes in co-nonsolvency behavior of similar PNIPAM analogues.[28]

Cosolvent identity and content significantly alter the micellar assembly observed in aqueous solutions of blocky-functionalized copolymers. Ethanol incorporation up to 5% leads to dramatically smaller aggregate sizes vs. homopolymers or random copolymers, suggesting that the assembly effect is still quite strong at these EtOH concentrations; the same level of DMF incorporation does not alter the initial aggregate size, suggesting that polymer-solvent interactions are more critical to determining the aggregate size than polymer architecture. This assembly effect is most predominant in water-rich systems, as higher concentrations of both ethanol and DMF lead to larger and more disperse structures formed above T_{CP}. However, even in systems where the initial D_h and *PDI* (before cycling) are similar for a blocky-functionalized copolymer and a homopolymer control, the copolymer displays distinct optical responses. Upon cycling, the minimum transmittance at high T decreases for systems containing up to 5% mol ethanol or DMF (Figs. 5, 10a) – likely corresponding to a de-

crease in structure size as evidenced by DLS (Fig. S18). Thus while the initial micellar assembly is not as strong in cosolvent-containing systems, the architecture of the blocky-functionalized polymers leads to a characteristic reduction in structure size upon cycling, and therefore increased transmittance above T_{CP}. This behavior occurs because intermolecular crosslinking is limited to one portion of the chain, thus covalent structure preservation only occurs when TMA-containing blocks are adjacent to one another. This structure preservation process appears to take several cycles, as aggregates may need to re-form several times before TMA-containing ends are adjacent and can crosslink. However, additional crosslinking that can occur with each subsequent thermal cycle diminishes as a 'stable' structure size is approached, evidenced by the smaller increases in transmittance with increasing cycle number (Figs. 5, 10a). Thus even in systems with high DMF content where the initial aggregate size is not influenced by polymer architecture, both cosolvent identity and polymer architecture are likely important for determining the stable aggregate size upon cycling. In any event, these results demonstrate that even though cosolvent incorporation can impact micellar assembly of blocky-functionalized copolymers, this polymer architecture provides a versatile route for accessing good thermoreversibility in systems requiring crosslinking moieties.

While the effects of cosolvent incorporation strongly depend on the cosolvent species, these results highlight the versatility of incorporating organic solvents to tune the properties of stimuli-responsive polymers. By small incorporations of ethanol ($\leq$5% mol), the transition temperatures can be tuned by $\sim$10 °C and the structure sizes formed above the transition temperature can be tuned by a nearly a factor of two. TMA incorporation these systems can enable crosslinked responsive particles of tunable size by varying the cosolvent content – even when the same starting polymers are used (SI.2.3). This control over structure size increases the utility of these polymers in applications such as drug delivery and sensing, where the surface area governs the function of the system.[11,75] Additionally, the conformation of polymers during processing onto surfaces can have a profound impact on the properties of the functionalized surface;[46] thus, cosolvent incorporation during coating processes could widen the application window of responsive surfaces. In summary, cosolvent incorporation into aqueous solutions of silane-functionalized thermoresponsive polymers can significantly alter the nanoscale structures formed across the LCST boundary, leading to distinct and tunable responses. This tunability can increase versatility of responsive polymers in applications requiring precise control over the transition temperatures and the structure size/uniformity, including sensing and drug delivery.

4 Conclusions

Thermoresponsive poly(*N*-isopropyl acrylamide) (PNIPAM) copolymerized with 3-(trimethoxysilyl)propyl methacrylate (TMA) can be used to generate covalently bonded polymeric nanostructures in aqueous systems; however, the tunability of the thermal and optical responses is limited. Here, organic cosolvent incorporation was shown to be an effective route for widely adjusting the critical temperatures, optical responses, and nanostructure formation across the lower critical solution temperature phase boundary in aqueous P(NIPAM-*co*-TMA). In the water-rich regime of polymer/water/ethanol systems, a configuration-dependent structure size is observed. PNIPAM homopolymers and random P(NIPAM-*co*-TMA) display a local minimum in hydrodynamic diameter (D_h) above T_{CP} at 2% mol ethanol. Conversely, blocky-functionalized polymers – which assemble into micelles at high temperatures in water – display a monotonic increase in structure size with increasing ethanol content but still retain uniform micellar structures. Ethanol incorporation primarily tunes the optical transition temperature and alters the minimum transmittance at high temperatures, corresponding with changes in hydrodynamic diameter D_h. For *N,N*-dimethyl formamide (DMF), substantially higher organic content can be incorporated without dramatically decreasing the transition temperatures. In contrast to ethanol-containing systems, a synergistic effect between DMF and TMA content is observed, leading to lower cloud point temperatures T_{CP} in polymers with higher TMA functionalization in systems with greater DMF content. This phenomenon is likely due to the decrease in hydrogen bonding between the polymer and the solvent with increasing TMA. Additionally, unique optical responses were observed at 15% mol DMF. This solvent composition corresponds to key transitions in the interactions between the polymer and solvent and the structure of the bulk solvent, likely leading to a more heterogeneous aggregate structure and reduced silane crosslinking. These findings can increase the versatility of thermoresponsive polymers in materials such as nanoparticles and structured coatings, as simple cosolvent addition can alter the structure size and thermal responses, leading to tunable behavior which can be leveraged in distinct applications.

Author Contributions

J.D.L. performed the experiments, performed analysis, and wrote the manuscript. F.A.R. assisted in initial screening of cosolvent systems, collecting cloud point data, and data analysis. M.A.C. supervised the research, performed analysis, and edited the manuscript.

Conflicts of interest

There are no conflicts to declare.

Acknowledgements

Researchers contributing to this work were supported by the Partnership for Research and Education in Materials (PREM) Program and the University of Minnesota MRSEC, funded by the National Science Foundation under Award Numbers DMR-2122178 and DMR-2011401 (F. Rodriguez). Any opinions, findings, and conclusions or recommendations expressed in this material are those of the authors and do not necessarily reflect the views of the National Science Foundation. NMR instruments used to collect data reported here was supported by the Office of the Director, National Institutes of Health, under Award Number S10OD011952. The content is solely the responsibility of the authors and does not necessarily represent the official views of the National Institutes of Health.

Notes and references

1 D. Roy, W. L. A. Brooks and B. S. Sumerlin, *Chemical Society Reviews*, 2013, **42**, 7214–7243.

2 M. Kaufmann, Y. Jia, L. Renner, S. Gupta, D. Kuckling, C. Werner and T. Pompe, *Soft Matter*, 2010, **6**, 937–944.

3 Abdullah-Al-Nahain, K. S. Lee, T. Mosaiab and S. Y. Park, *Journal of Applied Polymer Science*, 2013, **130**, 168–174.

4 S. Brahim, D. Narinesingh and A. Guiseppi-Elie, *Biomacromolecules*, 2003, **4**, 1224–1231.

5 S. Qian, S. Li, W. Xiong, H. Khan, J. Huang and W. Zhang, *Polymer Chemistry*, 2019, **10**, 5001–5009.

6 M. A. C. Stuart, W. T. S. Huck, J. Genzer, M. Müller, C. Ober, M. Stamm, G. B. Sukhorukov, I. Szleifer, V. V. Tsukruk, M. Urban, F. Winnik, S. Zauscher, I. Luzinov and S. Minko, *Nature Materials*, 2010, **9**, 101–113.

7 H. Wang, J. Yi, S. Mukherjee, P. Banerjee and S. Zhou, *Nanoscale*, 2014, **6**, 13001–13011.

8 P. Eskandari, Z. Abousalman-Rezvani, S. Hajebi, H. Roghani-Mamaqani and M. Salami-Kalajahi, *European Polymer Journal*, 2020, **135**, 109877.

9 F. F. Sahle, M. Giulbudagian, J. Bergueiro, J. Lademann and M. Calderón, *Nanoscale*, 2017, **9**, 172–182.

10 C.-W. Lee, H.-S. Park, J.-G. Kim and M.-S. Gong, *Macromolecular Research*, 2005, **13**, 96–101.

11 M. Matsuguchi and S. Fujii, *Sensors*, 2018, **18**, 3283.

12 D.-M. Han, Q. Matthew Zhang and M. J. Serpe, *Nanoscale*, 2015, **7**, 2784–2789.

13 J.-J. Ding, J. Zhu, Y.-X. Li, X.-Q. Liu and L.-B. Sun, *Industrial & Engineering Chemistry Research*, 2017, **56**, 4341–4349.

14 E. Y. Kozhunova, G. A. Komarova, M. V. Anakhov, R. A. Gumerov and I. I. Potemkin, *ACS Applied Materials & Interfaces*, 2022, **14**, 57244–57250.

15 X. Xu, N. Bizmark, K. S. S. Christie, S. S. Datta, Z. J. Ren and R. D. Priestley, *Macromolecules*, 2022, **55**, 1894–1909.

16 M. Heskins and J. E. Guillet, *Journal of Macromolecular Science: Part A - Chemistry*, 1968, **2**, 1441–1455.

17 A. J. Convertine, B. S. Lokitz, Y. Vasileva, L. J. Myrick, C. W. Scales, A. B. Lowe and C. L. McCormick, *Macromolecules*, 2006, **39**, 1724–1730.

18 K. Nothdurft, D. H. Müller, S. D. Mürtz, A. A. Meyer, L. P. B. Guerzoni, A. Jans, A. J. C. Kühne, L. De Laporte, T. Brands, A. Bardow and W. Richtering, *The Journal of Physical Chemistry B*, 2021, **125**, 1503–1512.

19 K. Zielińska, H. Sun, R. A. Campbell, A. Zarbakhsh and M. Resmini, *Nanoscale*, 2016, **8**, 4951–4960.

20 D. Yang, H. Eronen, H. Tenhu and S. Hietala, *Langmuir*, 2021, **37**, 2639–2648.

21 S. Sbeih, P. S. Mohanty, A. Yethiraj and M. R. Morrow, *Langmuir*, 2021, **37**, 13664–13675.

22 B. P. Rosi, L. Tavagnacco, L. Comez, P. Sassi, M. Ricci, E. Buratti, M. Bertoldo, C. Petrillo, E. Zaccarelli, E. Chiessi and S. Corezzi, *Journal of Colloid and Interface Science*, 2021, **604**, 705–718.

23 Z. Osváth, T. Tóth and B. Iván, *Macromolecular Rapid Communications*, 2017, **38**, 1600724.

24 S. K. Kang, D. H. Ho, C. H. Lee, H. S. Lim and J. H. Cho, *ACS Applied Materials & Interfaces*, 2020, **12**, 33838–33845.

25 S. T. Jones, Z. Walsh-Korb, S. J. Barrow, S. L. Henderson, J. del Barrio and O. A. Scherman, *ACS Nano*, 2016, **10**, 3158–3165.

26 S. R. Deka, A. Quarta, R. Di Corato, A. Riedinger, R. Cingolani and T. Pellegrino, *Nanoscale*, 2011, **3**, 619–629.

27 W. Li, L. Hu, J. Zhu, D. Li, Y. Luan, W. Xu and M. J. Serpe, *ACS Applied Materials & Interfaces*, 2017, **9**, 26539–26548.

28 C. Henschel, D. Schanzenbach, A. Laschewsky, C.-H. Ko, C. M. Papadakis and P. Müller-Buschbaum, *Colloid and Polymer Science*, 2023, **301**, 703–720.

29 M. Matsuguchi and A. Tada, *Sensors and Actuators B: Chemical*, 2017, **251**, 821–827.

30 M. Gaumet, A. Vargas, R. Gurny and F. Delie, *European Journal of Pharmaceutics and Biopharmaceutics*, 2008, **69**, 1–9.

31 M. Bagheri, J. Bresseleers, A. Varela-Moreira, O. Sandre, S. A. Meeuwissen, R. M. Schiffelers, J. M. Metselaar, C. F. van Nostrum, J. C. M. van Hest and W. E. Hennink, *Langmuir*, 2018, **34**, 15495–15506.

32 J. D. Linn, L. Liberman, C. A. P. Neal and M. A. Calabrese, *Polymer Chemistry*, 2022, **13**, 3840–3855.

33 A. A. A. Smith, C. L. Maikawa, H. Lopez Hernandez and E. A. Appel, *Polymer Chemistry*, 2021, **12**, 1918–1923.

34 I. Akar, J. C. Foster, X. Leng, A. K. Pearce, R. T. Mathers and R. K. O'Reilly, *ACS Macro Letters*, 2022, **11**, 498–503.

35 M. C. Costa, S. M. Silva and F. E. Antunes, *Journal of Molecular Liquids*, 2015, **210**, 113–118.

36 A. Pica and G. Graziano, *Polymer*, 2017, **124**, 101–106.

37 T. Patel, G. Ghosh, S.-i. Yusa and P. Bahadur, *Journal of Dispersion Science and Technology*, 2011, **32**, 1111–1118.

38 *Liquid film coating: scientific principles and their technological implications*, ed. S. F. Kistler, Chapman & Hall, London Weinheim, 1st edn, 1997, pp. 495 – 536.

39 A. Roy, A. Ghosh, S. Datta, S. Das, P. Mohanraj, J. Deb and M. Bhanoji Rao, *Saudi Pharmaceutical Journal*, 2009, **17**, 233–241.

40 Y. Qiang, S. Zhang, S. Yan, X. Zou and S. Chen, *Corrosion Science*, 2017, **126**, 295–304.

41 R. O. Costa and R. F. Freitas, *Polymer*, 2002, **43**, 5879–5885.

42 I. Bischofberger, D. C. E. Calzolari, P. De Los Rios, I. Jelezarov and V. Trappe, *Scientific Reports*, 2014, **4**, 4377.

43 S. Bharadwaj, B.-J. Niebuur, K. Nothdurft, W. Richtering, N. F. A. van der Vegt and C. M. Papadakis, *Soft Matter*, 2022, **18**, 2884–2909.

44 M. D. Morales-Moctezuma and S. G. Spain, *Polymer Chemistry*, 2021, **12**, 4696–4706.

45 H. Tokuyama, N. Ishihara and S. Sakohara, *Polymer Bulletin*, 2008, **61**, 399–405.

46 T. Yakushiji, K. Sakai, A. Kikuchi, T. Aoyagi, Y. Sakurai and T. Okano, *Langmuir*, 1998, **14**, 4657–4662.

47 Y. Yu, R. A. Lopez De La Cruz, B. D. Kieviet, H. Gojzewski,

A. Pons, G. Julius Vancso and S. De Beer, *Nanoscale*, 2017, **9**, 1670–1675.
48 Y.-M. Sun, W. Wang, Y.-Y. Wei, N.-N. Deng, Z. Liu, X.-J. Ju, R. Xie and L.-Y. Chu, *Lab Chip*, 2014, **14**, 2418–2427.
49 H. Wei, C. Cheng, C. Chang, W.-Q. Chen, S.-X. Cheng, X.-Z. Zhang and R.-X. Zhuo, *Langmuir*, 2008, **24**, 4564–4570.
50 H. Wei, R. Ravarian, S. Dehn, S. Perrier and F. Dehghani, *Journal of Polymer Science Part A: Polymer Chemistry*, 2011, **49**, 1809–1820.
51 V. Mellon, D. Rinaldi, E. Bourgeat-Lami and F. D'Agosto, *Macromolecules*, 2005, **38**, 1591–1598.
52 A. L. B. Maçon, S. L. Greasley, C. R. Becer and J. R. Jones, *Macromolecular Rapid Communications*, 2015, **36**, 2060–2064.
53 B. V. K. J. Schmidt, M. Hetzer, H. Ritter and C. Barner-Kowollik, *Macromolecules*, 2011, **44**, 7220–7232.
54 C. A. P. Neal, V. León, M. C. Quan, N. O. Chibambo and M. A. Calabrese, *J. Colloid Interface Sci.*, 2023, **629**, 878–895.
55 F. I. El-Dossoki, *Journal of the Chinese Chemical Society*, 2007, **54**, 1129–1137.
56 T. A. Scott, *The Journal of Physical Chemistry*, 1946, **50**, 406–412.
57 M. Yusa, G. P. Mathur and R. A. Stager, *Journal of Chemical & Engineering Data*, 1977, **22**, 32–35.
58 S. Taniewska-Osinska, A. Piekarska and A. Kacperska, *Journal of Solution Chemistry*, 1983, **12**, 717–727.
59 C. A. P. Neal, G. V. Kresge, M. C. Quan, V. León, N. O. Chibambo and M. A. Calabrese, *Journal of Vinyl and Additive Technology*, 2023, **29**, 795–812.
60 I. Bischofberger, D. C. E. Calzolari and V. Trappe, *Soft Matter*, 2014, **10**, 8288–8295.
61 M. J. A. Hore, B. Hammouda, Y. Li and H. Cheng, *Macromolecules*, 2013, **46**, 7894–7901.
62 C. H. Lee and Y. C. Bae, *Polymer*, 2020, **195**, 122428.
63 S. Bharadwaj, P. B. Sunil Kumar, S. Komura and A. P. Deshpande, *The Journal of Chemical Physics*, 2018, **148**, 084903.
64 S. Bharadwaj, D. Nayar, C. Dalgicdir and N. F. A. Van Der Vegt, *Communications Chemistry*, 2020, **3**, 165.
65 L. Tavagnacco, E. Zaccarelli and E. Chiessi, *Journal of Molecular Liquids*, 2020, **297**, 111928.
66 T. Zuo, C. Ma, G. Jiao, Z. Han, S. Xiao, H. Liang, L. Hong, D. Bowron, A. Soper, C. C. Han and H. Cheng, *Macromolecules*, 2019, **52**, 457–464.
67 A. Issa and A. Luyt, *Polymers*, 2019, **11**, 537.
68 Z. Osváth, T. Tóth and B. Iván, *Polymer*, 2017, **108**, 395–399.
69 P.-w. Zhu and L. Chen, *Physical Review E*, 2019, **99**, 022501.
70 Z. Osváth and B. Iván, *Macromolecular Chemistry and Physics*, 2017, **218**, 1600470.
71 Q. Zhang, P. Schattling, P. Theato and R. Hoogenboom, *Polymer Chemistry*, 2012, **3**, 1418.
72 B. Yang, H. Lang, Z. Liu, S. Wang, Z. Men and C. Sun, *Journal of Molecular Liquids*, 2021, **324**, 114996.
73 I. Bischofberger and V. Trappe, *Sci. Rep.*, 2015, **5**, 15520.
74 M. Jóźwiak, A. Burakowski, M. Tyczyńska and M. Komudzińska, *Journal of Molecular Liquids*, 2022, **362**, 119722.
75 M. Danaei, M. Dehghankhold, S. Ataei, F. Hasanzadeh Davarani, R. Javanmard, A. Dokhani, S. Khorasani and M. Mozafari, *Pharmaceutics*, 2018, **10**, 57.